Temperature and Surface Charge Effects on Clay-Water Contact Angle: A Molecular Dynamics Study

Yu Zhong[1], Annan Zhou[*,1]

[1]*Discipline of Civil and Infrastructure Engineering, School of Engineering, Royal Melbourne Institute of Technology (RMIT), Victoria 3001, Australia*

[*]*Corresponding author's email:* annan.zhou@rmit.edu.au

Abstract: The clay-water contact angle emerges as a pivotal parameter essential for elucidating various engineering challenges. Its variability is closely linked to surface charge and ambient temperature, but current research on their joint effects is incomplete, lacking insights from molecular dynamics (MD) perspective. This study has established diverse montmorillonite-water systems under varying surface charge conditions (cation exchange capacity = 0, 27.60, 54.84, 108.38, and 134.73 meq/100g) and ambient temperatures (277, 293, 313, 353, 393, and 433 K) through the MD method. The liquid phase boundary is determined by extracting density contour plots and a unified conical curve is introduced to quantitatively analyze the contact angle. This approach led to the development of a nonlinear equation for estimating contact angle variations under different surface charges and ambient temperatures. Finally, the proposed equation is validated against literature data, which exhibits remarkable accuracy in predicting the variations of contact angles induced by ambient temperature under various surface charge conditions. These findings offer valuable insights and practical equation for designing clay impermeable layers in engineering applications.

1. Introduction

The contact angle is an important concept with widespread applications in various fields. It describes the angle at which a liquid contacts a solid surface, directly reflecting the properties of the solid-liquid interface. Changes in the contact angle may lead to engineering problems that often result in severe consequences, including loss of life, such as slope erosion due to rainfall infiltration [1]. Therefore, understanding the factors influencing the contact angle and the underlying mechanisms is crucial for designing various engineering applications. Clayey soil is often used to address complex engineering problems considering its good adsorption properties and low permeability, and the clay-water contact angle emerges as a pivotal parameter essential for these engineering applications. Shang, et al. [2] observed the deviations in contact angles for the same clay, ranging from 10° to 40°, indicating the impact of measurement methods on clay-water contact angles has not been comprehensively quantified.

It has been acknowledged that clay is primarily composed of minerals like montmorillonite that is sensitive to the external environment, and the wettability of clay surface is significantly affected by temperature changes. Su, et al. [3] reported a gradual reduction in the contact angle on montmorillonite surfaces with increasing temperature. In contrast, Liu, et al. [4] discovered that high temperatures diminish the surface aluminum elements and hydroxyl groups on montmorillonite, altering its layered structure. This modification leads to a decrease in surface negative charge and hydrophilicity, resulting in an increase in contact angle (from 7.4° at 25 °C to 15.7° at 200 °C), which diverges from the trends reported in other studies.

The current confusion on montmorillonite surface contact angles is mainly due to the failure to consider the joint effects of surface charge and ambient temperature on contact angle. Moreover, the measured contact angle is also related to experimental conditions, but maintaining precise control over structural morphology, component ratios, and experimental conditions during measurement presents a significant challenge in laboratory settings. With a deeper understanding of this field, molecular dynamics (MD) methods have emerged as effective tools for investigating interfacial issues like the variation in contact angles. Szczerba, et al. [5] pointed out that ion-free montmorillonite surfaces exhibit hydrophobic or moderately hydrophilic characteristics, with highly hydrophilic properties observed in experiments primarily due to surface charge-balancing cations. Therefore, ions on the montmorillonite surface play a critical role in adsorbing water molecules, thereby affecting wettability. The ion presence is reflected as surface charge, which can be generally quantified by Cation Exchange Capacity (CEC), where higher CEC corresponds to increased surface ion content and activity, and lower CEC has the opposite effect. Thus, accurately predicting the changes in contact angles between clay and water under different ambient temperature and surface charge conditions is crucial to address engineering challenges related to hydraulic characteristics.

This paper established a series molecular model to simulate static contact angles under different ambient temperature and surface charge conditions (CEC) and proposed a functional correlation among them for practical application, which is validated by reported data in literature. In-depth discussion and analysis on the evolution of clay contact angles in response to temperature and CEC variations are also presented.

2. Methodology

2.1 Static contact angle

On an ideally smooth surface, the contact angle is governed exclusively by the surface properties, meaning that the three-phase point satisfies Young's Equation: $\gamma_{sv} = \gamma_{sl} + \gamma_{lv} \cos\theta$, where γ_{sv}, γ_{sl} and γ_{lv} are the surface tension (N/m) between solid-vapor, solid-liquid, and liquid-vapor, respectively. θ is the static contact angle (degree) as shown in Fig. 1, and our research focuses on exploring its response to varying ambient temperature and surface charge conditions.

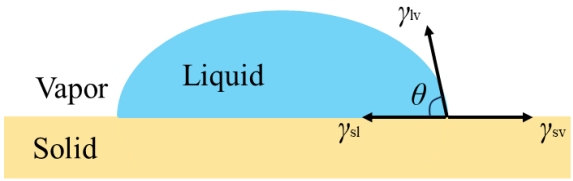

Figure 1 Diagram of static contact angle.

2.2 Model establishment and simulation parameters

This structure of clay minerals involves layers of silicon-oxygen tetrahedra and aluminum-hydroxide octahedra, as shown in Fig. 2. This study focuses on montmorillonite due to its pronounced surface interactions, aiming to provide a more comprehensive understanding of its applications. The lattice parameters of Na-montmorillonite are as follows: a = 5.18 Å, b = 8.98 Å, c = 15.00 Å, with angles $\alpha = \beta = \gamma = 90.0°$. To create an adequate surface area, we replicate the unit cell 5 times along the x-axis and 22 times along the y-axis. The overall model dimensions are 25.90 × 197.56 × 250.00 Å, which includes a 100 Å vacuum layer to ensure sufficient space for bulk water placement. After constructing the basic structure, aluminum (Al) and magnesium (Mg) atoms are randomly substituted for silicon (Si) and aluminum (Al) atoms within the montmorillonite lattice, creating a negatively charged surface. Sodium ions are then added to neutralize this charge, resulting in models with varying CEC values (0, 27.60, 54.84, 108.38 and 134.73 meq/100g). Upon completion of the layer, a cuboid-shaped bulk water with a density of 1.0 g/cm^3 and dimensions of 25.90 × 50.00 × 50.00 Å is introduced into the system.

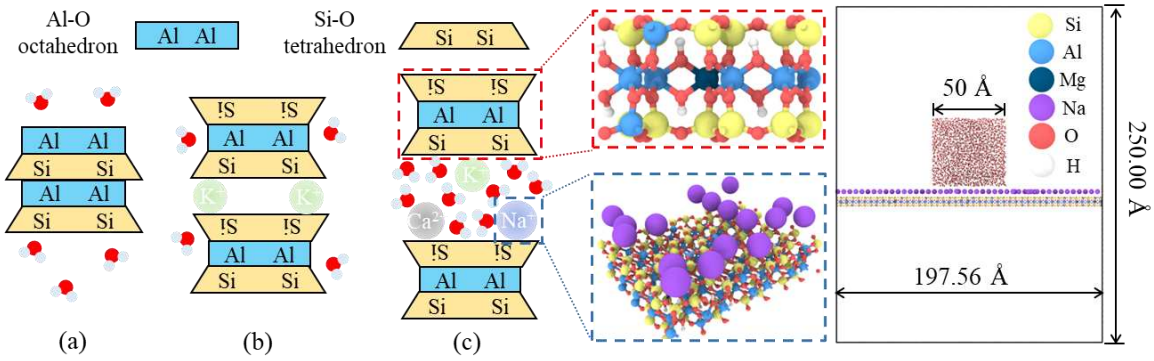

Figure 2: Diagram of three types of clay minerals. (a) Kaolinite; (b) Illite; (c) Montmorillonite and the corresponding MD model.

2.3 Simulation process

After establishing the MD model, we employed the Clayff force field [6] to calculate the influences of different temperatures and CEC values on the contact angles in montmorillonite-

water systems. All the calculation parameters can be obtained from previous research done by Cygan, et al. [6] and will not be further elaborated here. We conducted simulations across five different initial CEC models, subjecting them to six predefined temperatures ranging from 277 K to 433 K (277, 293, 313, 353, 393 and 433 K). The 30 MD simulation cases were conducted by using the Large-scale Atomic/Molecular Massively Parallel Simulator (LAMMPS) [7]. The simulation time step is set to 1 fs, with an interaction cutoff radius of 12 Å. We employed the 99.99% PPPM method for calculating long-range electrostatic forces. The clay layer was fixed to enhance computation efficiency, allowing only the sodium ions and water molecules to move freely on its surface. Subsequently, the system was relaxed for 100 ps under the NVT ensemble to eliminate unreasonable configurations and achieve a state of relative equilibrium. After relaxation, the entire system was divided into 1 × 1 Å^2 strips in the *y*-*z* plane to facilitate data collection. Water density within each strip was sampled every 10 fs and averaged every 1 ns.

3. Simulation results analysis

3.1 Contact angle calculation

We consider strip densities in the range of 0.4-0.5 g/cm^3 [8] as indicative of the boundary density, and the coordinates of these strips are then recorded to determine the corresponding boundary points, as shown in Table 1. The conic equation is commonly used to fit the calculated contact angles at the solid-liquid interface [9]. Therefore, the unified conic curve equation is applied first to fit the derived boundary points of the water phase:

$$(1 - e^2)y^2 + z^2 - 2pe^2y - p^2e^2 = C \tag{1}$$

where e and p are eccentricity and directrix position (dimensionless), respectively; C is an arbitrary constant (dimensionless).

Table 1: The density contour plot and extracted water boundary of representative cases

	0 meq/100g	134.73 meq/100g
277 K	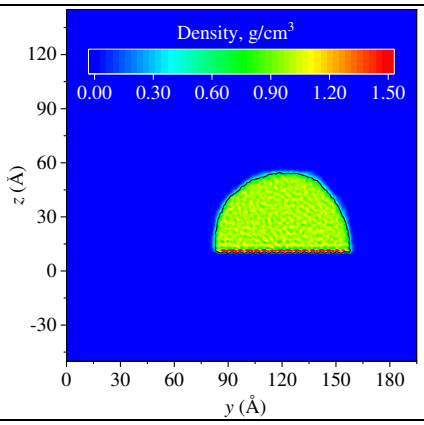	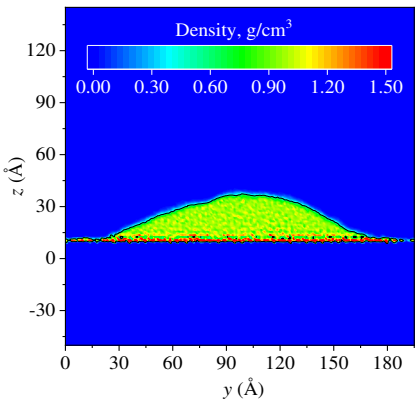

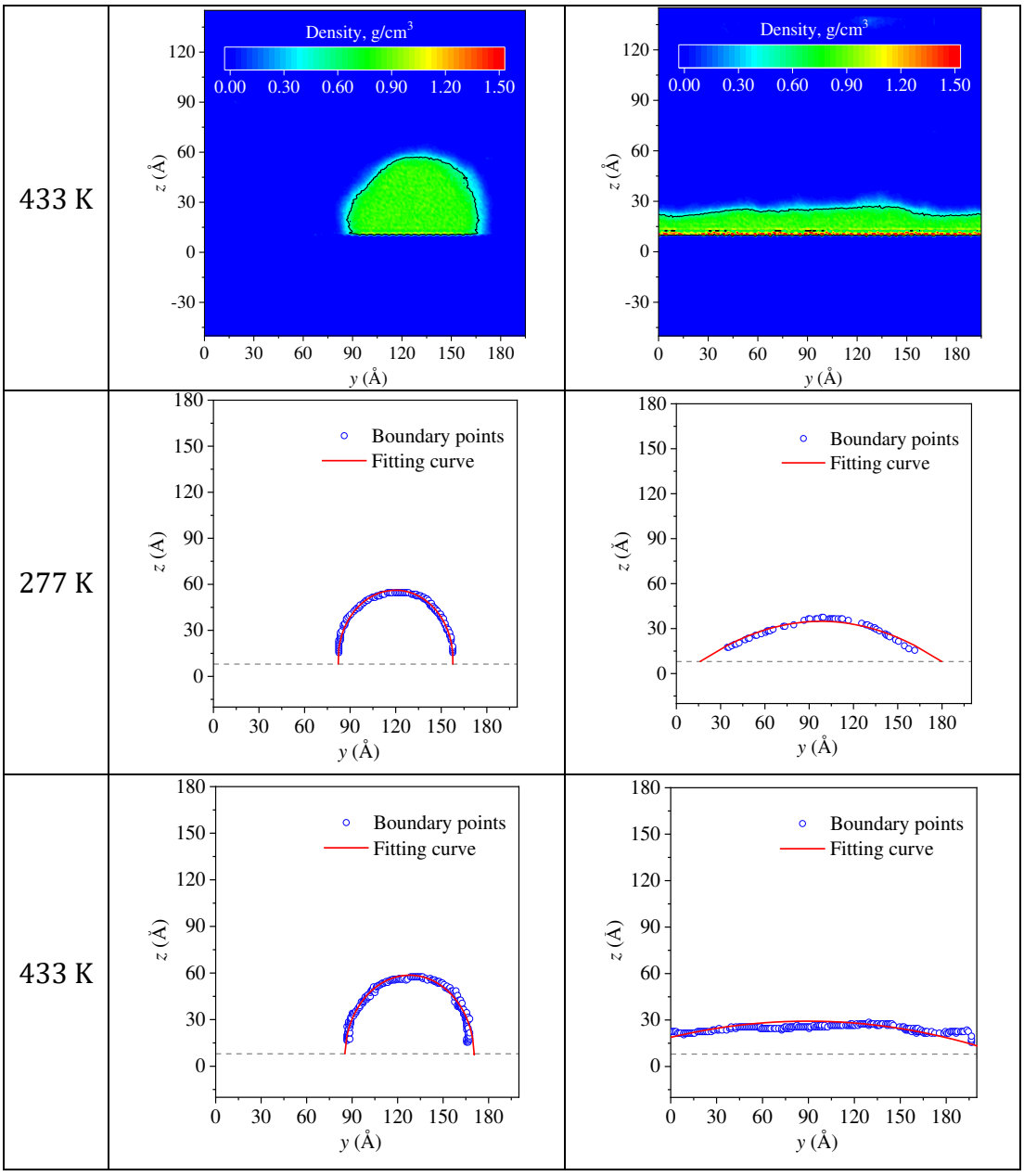

Table 2: The calculated contact angle (degree) of different cases

CEC (meq/100g)		0	27.60	54.84	108.38	134.73
Temperature, *T* (K)	277	93.29	49.59	33.51	30.83	33.23
	293	89.47	46.43	28.89	25.71	29.71
	313	90.87	41.21	28.83	28.69	27.98
	353	90.21	39.12	30.80	25.10	22.75
	393	91.08	38.42	28.96	22.44	24.85
	433	88.46	41.35	28.84	21.79	19.16

3.2 Influence of temperature and CEC on the contact angle

Table 2 shows how contact angles vary with CEC under different temperatures. To quantify the relationship among them, we utilized a nonlinear fitting method and got the following equation: $\theta = A_1 \exp\left(-\frac{CEC}{A_2}\right) + A_3$, where A_1, A_2 and A_3 are the fitting parameters. The units of A_1 and A_3 are the same as the contact angle (degree), and Fig. 3 reveals that A_1 increases with temperature, whereas A_3 shows a decreasing trend with temperature. A_2, as the normalization factor for CEC (meq/100g), is almost constant fluctuating around 20, which can be reasonably approximated by its average value of 20.51 meq/100g. As shown in Fig. 3, both A_1 and A_3 exhibit robust linear correlations with temperature, evidenced by R-squared values of 0.98 and 0.88. This leads to an empirical equation of comprehensive relationship involving contact angles (θ), CEC, and temperature (T):

$$\theta = (0.039T + 51.50)\exp\left(-\frac{CEC}{20.51}\right) - 0.057T + 45.33 \quad (2)$$

where T is the temperature (K).

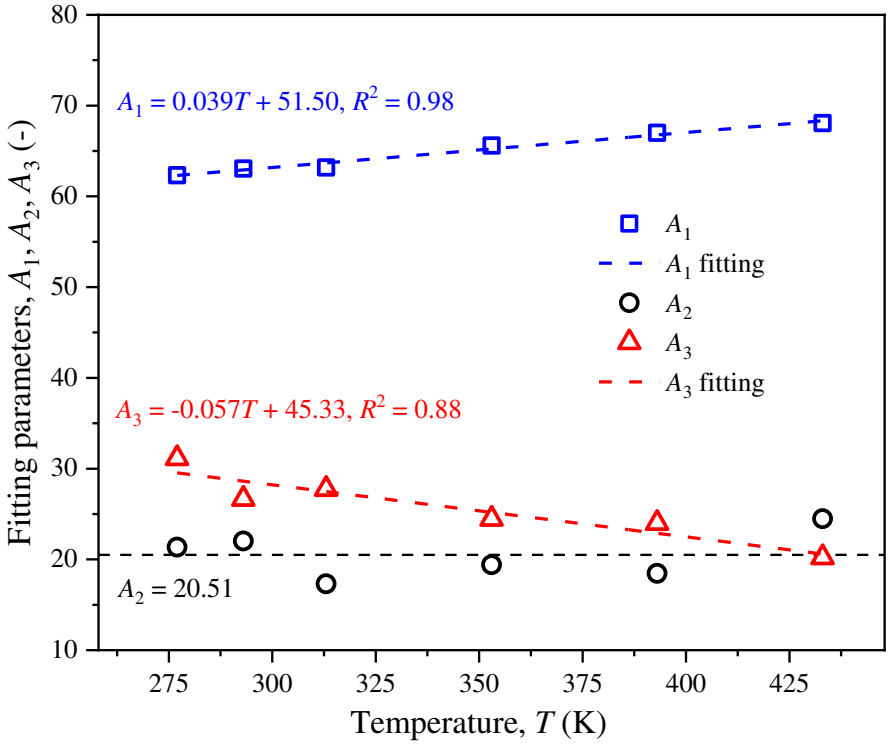

Figure 3: The relationship between fitting parameters A_1, A_2, A_3, and temperature.

4. Verification and discussion

4.1 Verification

The validation of our contact angle calculation model, as represented by Eq. (2), is conducted through a comparative analysis with experimental data sourced from relevant literature [3, 10-15], which are presented in Fig. 4. Fig. 4(a) demonstrates the model's ability to accurately capture the trend of decreasing contact angles with increasing temperature, achieving a correlation coefficient of 0.92 across the entire temperature range. Moreover, as shown in Fig. 4(b), the experimental contact angles for montmorillonite at room-temperature reported by different researchers range between 20-38°. In comparison, our model estimates an average contact angle of around 28°, which well falls within the range of experimental data and demonstrates its effectiveness. It should be noted that the high CEC value of montmorillonite results in strong hydrophilicity, which in turn complicates the experimental extraction of the three-phase contact point. This complexity contributes to the fluctuations observed in experimental measurements. In contrast, our model yields stable and consistent results, providing a reliable reference for engineering calculations, such as infiltration and permeation.

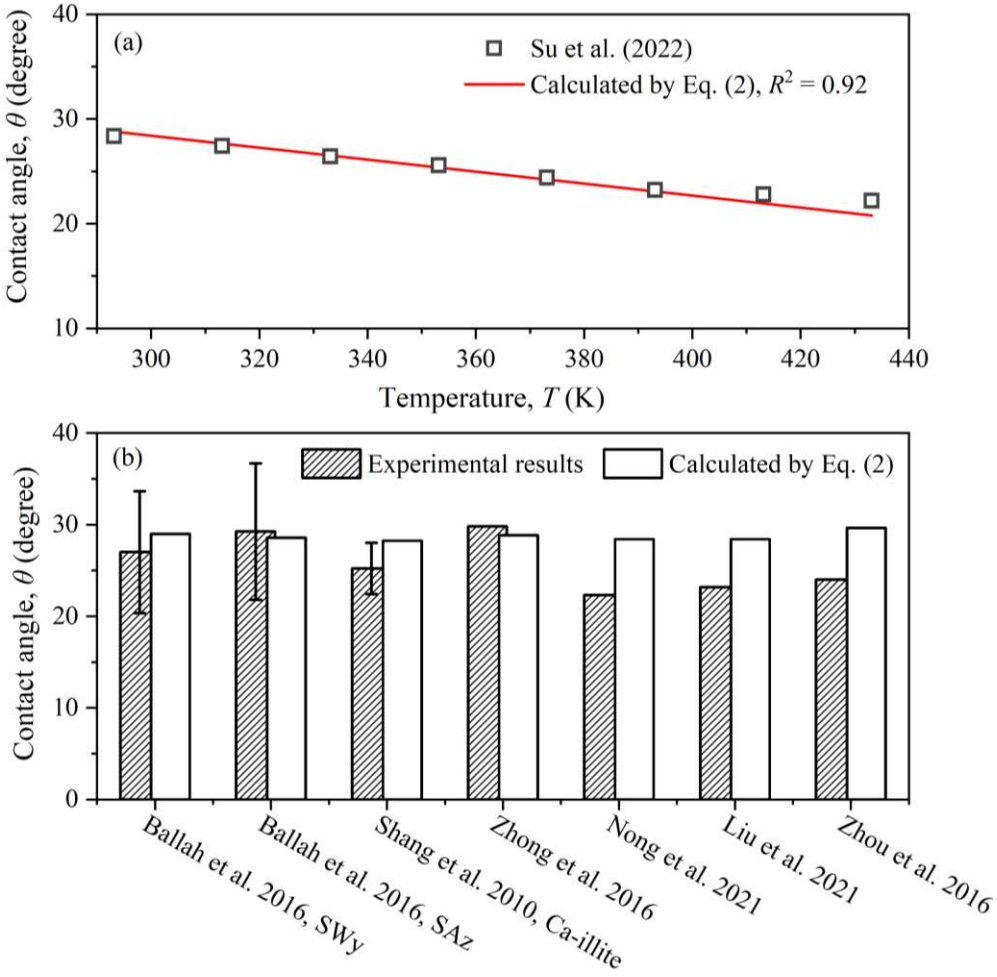

Figure 4: Comparison of literature experimental data and computational data.

4.2 Discussion and implication

Fig. 5(a) shows the 3D contour plot of the contact angle between montmorillonite and water at different CEC levels and temperatures. It is noteworthy that the consistent decrease in contact angle with the concurrent rise in both temperature and CEC, with the maximum variation reaching approximately 70°. An analysis of six representative CEC values, as presented in Fig. 5(b), reveals a linear relationship between contact angle and temperature. As the CEC increases from the neutral condition (CEC = 0), hydrophilicity of montmorillonite surface is progressively strengthened. However, beyond a CEC threshold of 80 meq/100g, its effect on the contact angle gradually reaches a stable stage, at which temperature becomes the primary factor.

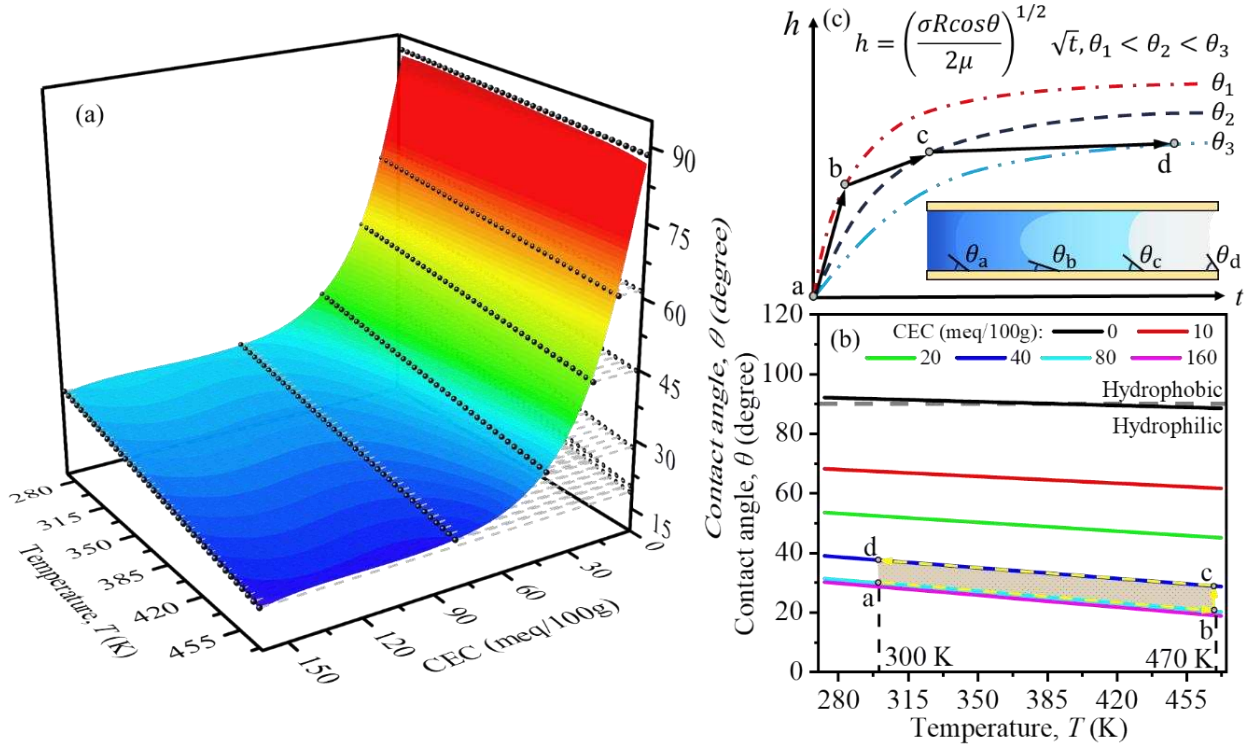

Figure 5: Dependence of clay-water contact angle of CEC and temperature and its implication to design of clay barrier layer for nuclear waste disposal. (a) Three-dimensional relationship diagram of contact angle (θ), CEC, and temperature (T); (b) Extracted six representative CEC cases and the variation path of the contact angle (a→b→c→d); (c) The variation of infiltration height and contact angle during the entire decay period of nuclear waste.

In the context of nuclear waste disposal, the CEC of clay barrier layer can undergo significant variations, as evidenced by reductions from approximately 80 to 50 meq/100g [16], influenced by radioactive radiation. This change directly affects the clay's impermeability, with the impact on the contact angle observed in Fig. 5(b). When nuclear waste is disposed of within a clay protective barrier (point a), the substantial thermal energy generated by fission decay increases the barrier's temperature, causing a continuous decrease in the contact angle until it stabilizes at a new equilibrium (point b). In this state, the combined effects of temperature and energy

from nuclear radiation continue to affect the clay, resulting in the illitization of montmorillonite, which decreases its surface charge (point c). As radioactive decay progresses, the temperature gradually drops, leading to an increase in the contact angle (point d). The performance of the clay protective barrier can be assessed using the infiltration height and matrix suction, governed by the following equations: $h = \left(\frac{\sigma R\cos\theta}{2\mu}\right)^{1/2}\sqrt{t}$ and $s = \frac{2\sigma\cos\theta}{R}$, where h is the infiltration height (m); σ is the surface tension (N/m); R is the pore radius (m); μ is the viscosity (Pa·s); t is time (s); s is matrix suction (Pa).

The equations indicate that both infiltration height and matrix suction are directly related to the contact angle, decreasing as the contact angle increases. The contact angle trajectory a→b→c→d in Fig. 5(b) corresponds to the evolution of infiltration height, as depicted in Fig. 5(c). In Fig. 5(c), θ_1, θ_2, and θ_3 represent the calculated results of selected contact angles ($\theta_1 < \theta_2 < \theta_3$), while θ_a, θ_b, θ_c, and θ_d correspond to contact angles at points a, b, c, and d in Fig. 5(b). For convenience, we assume $\theta_a=\theta_c=\theta_2$, $\theta_b=\theta_1$, and $\theta_d=\theta_3$. The solid black line represents the modified trend of infiltration height. From a to b, as the temperature rises and the contact angle decreases, matrix suction increases, leading to a higher infiltration rate and greater infiltration length compared to the initial state. From b to c, the reduction in contact angle due to a decrease in CEC lowers matrix suction, slowing the infiltration rate and stabilizing the infiltration length. From c to d, as the temperature drops and the contact angle increases, matrix suction decreases, and the infiltration height remains relatively stable. Considering the fluctuation of CEC in a radiation environment (around 30 meq/100g), designing clay protective layers with a CEC value of about 110 meq/100g is advisable to ensure protective layer stability.

5. Conclusion

Through MD simulations, we have explored the impacts of surface charge (CEC) and ambient temperature on the contact angle of montmorillonite. The key findings are as follows:

1. A nonlinear fitting process was conducted to evaluate the impact of CEC and temperature on contact angles, resulting in a cost-effective evaluation model. The effectiveness of the proposed model is further validated by comparisons with data from relevant literature.

2. Our analysis indicates that CEC predominates in influencing the contact angle when it is below 80 meq/100g, which is crucial for nuclear waste disposal scenarios to mitigate the risk of project failures due to CEC variations.

Further Information

For a more comprehensive discussion and additional details, please refer to the full version of this paper: Y. Zhong, A. Zhou, J. Du, and S. Zhan. Dependence of clay–water contact angle on surface charge and ambient temperature: A study from molecular dynamics perspective. *Journal of Molecular Liquids*, *415*, 126258, 2024. doi.org/10.1016/j.molliq.2024.126258

References

[1] R. Morbidelli, C. Saltalippi, A. Flammini, and R. S. Govindaraju. Role of slope on infiltration: A review. *Journal of Hydrology,* 557: 878-886, 2018.

[2] J. Shang, M. Flury, J. B. Harsh, and R. L. Zollars. Comparison of different methods to measure contact angles of soil colloids. *Journal of Colloid and Interface Science,* 328(2): 299-307, 2008.

[3] J. Su *et al.* Sulfonated lignin modified with silane coupling agent as biodegradable shale inhibitor in water-based drilling fluid. *Journal of Petroleum Science and Engineering,* 208: 109618, 2022.

[4] J. Liu, T. Zhang, Y. Sun, D. Lin, X. Feng, and F. Wang. Insights into the high temperature-induced failure mechanism of bentonite in drilling fluid. *Chemical Engineering Journal,* 445: 136680, 2022.

[5] M. Szczerba, A. G. Kalinichev, and M. Kowalik. Intrinsic hydrophobicity of smectite basal surfaces quantitatively probed by molecular dynamics simulations. *Applied Clay Science,* 188: 2020.

[6] R. T. Cygan, J. J. Liang, and A. G. Kalinichev. Molecular models of hydroxide, oxyhydroxide, and clay phases and the development of a general force field. *The Journal of Physical Chemistry B,* 108(4): 1255-1266, 2004.

[7] S. Plimpton. Fast Parallel Algorithms for Short-Range Molecular Dynamics. *Journal of Computational Physics,* 117: 1-19, 1995.

[8] R. Šolc, M. H. Gerzabek, H. Lischka, and D. Tunega. Wettability of kaolinite (001) surfaces—Molecular dynamic study. *Geoderma,* 169: 47-54, 2011.

[9] A. K. Giri and M. Sega. Instantaneous Fundamental Modes and Contact Angles of Droplets From Surface Atoms. *Journal of Molecular Liquids*: 125155, 2024.

[10] J. Ballah, M. Chamerois, S. Durand-Vidal, N. Malikova, P. Levitz, and L. Michot. Effect of chemical and geometrical parameters influencing the wettability of smectite clay films. *Colloids and Surfaces A: Physicochemical and Engineering Aspects,* 511: 255-263, 2016.

[11] L. Liu *et al.* Pickering emulsion stabilized by organoclay and intermediately hydrophobic nanosilica for high-temperature conditions. *Colloids and Surfaces A: Physicochemical and Engineering Aspects,* 610: 125694, 2021.

[12] Y. Nong, J. Sun, M. Fu, H. Chen, and Z. Zhang. Effects of cationic modifier type on the structure and morphology of organo-montmorillonite and its application properties in a high-temperature white oil system. *Applied Clay Science,* 203: 105995, 2021.

[13] J. Shang, M. Flury, J. B. Harsh, and R. L. Zollars. Contact angles of aluminosilicate clays as affected by relative humidity and exchangeable cations. *Colloids and Surfaces A: Physicochemical and Engineering Aspects,* 353(1): 1-9, 2010.

[14] H. Zhong, Z. Qiu, Z. Tang, X. Zhang, J. Xu, and W. Huang. Study of 4, 4′-methylenebis-cyclohexanamine as a high temperature-resistant shale inhibitor. *Journal of Materials Science,* 51: 7585-7597, 2016.

[15] D. Zhou, Z. Zhang, J. Tang, F. Wang, and L. Liao. Applied properties of oil-based drilling fluids with montmorillonites modified by cationic and anionic surfactants. *Applied Clay Science,* 121: 1-8, 2016.

[16] J. O. Lee and W. J. Cho. Hydrothermal behaviors and long-term stability of bentonitic buffer material. *Journal of Nuclear Fuel Cycle and Waste Technology,* 5(2): 145-154, 2007.